Feasibility of laser induced jets in needle free jet injections

Pankaj Rohilla, Jeremy Marston*

Department of Chemical Engineering, Texas Tech University, Lubbock, TX 79409, United States

ABSTRACT

This paper reports a detailed characterization of laser-induced micro-jets, including ex vivo experiments using skin as a target substrate to check the feasibility in terms of needle-free jet injection. The actuation technique comprised a Nd-YAG based laser system to superheat the liquid locally, which creates a pressure wave actuating the motion of the liquid as a jet. Typical jet speeds were ~ $\mathscr{O}(10^2)$ m/s and diameters ~ $\mathscr{O}(10^1$–$10^2)$ μm and Re ~ $\mathscr{O}(10^2$–$10^4)$. We studied the effect of various system parameters related to both geometry (e.g., capillary diameter, laser focal point) and fluid properties (e.g., viscosity). To advance the understanding of liquid delivery into tissue, transient penetration dynamics and dispersion patterns were studied. Stand-off distance, mechanical strength of the proxy gel, and laser pulse energy were also found to affect the penetration of liquid jets into the skin models.

1. Introduction

High-speed liquid microjets have multiple applications ranging from ink-jet printing to needle-free jet injections. For application in needle-free jet injections, liquid jet generated via different techniques should have good precision, reproducibility, and controllability. With these requirements in mind, many researchers have explored different actuation techniques. Recently, Tagawa et al. reported a novel technique to generate high-speed microjets (Tagawa et al., 2012; Peters et al., 2013). This technique involves focusing a laser pulse at a point inside the capillary filled with liquid with one end closed while keeping the other end open to air. Instant localized superheating leads to phase transition of the liquid at constant pressure to vapor phase, resulting in bubble generation (Brennen, 2014). As a result, a pressure wave is generated pushing liquid out of the capillary from the open end as a jet, which accelerates further due to the flow focusing phenomenon (Tagawa et al., 2016). Microjets of viscous liquids and non-Newtonian liquids have also been generated via the flow focusing technique in the past (Onuki et al., 2018; Kiyama et al., 2016; Yoh and Jang, 2016).

The focused jets observed by Tagawa et al. achieved high speeds up to 850 m/s for absorbed laser energy of $\mathscr{O}(10\,\mu J)$ (Tagawa et al., 2012). Other important features of these focused jets from the perspective of application in needle-free vaccine delivery are jet coherency (i.e., a slender collimated stream), good controllability and reproducibility (Park et al., 2012). In extension of this study, Tagawa et al. have used skin models such as hydrogels, rat skin, and artificial human skin for needle-free jet injection delivery (Tagawa et al., 2013; Kiyama et al.,

2019). However, these studies lack in-depth jet characterization and a good understanding of penetration dynamics along with liquid dispersion within the skin tissue.

In comparison to focused jets generated by pulsed laser technique, traditional jet injectors generate more diffused jets, as shown in Fig. 1 which presents a comparison of a focused jet generated via laser focusing technique and a diffuse jet generated with a spring based jet injector. Whilst the role of the shape of the jet has not been fully characterized, it was observed by Park et al. that dispersed jets led to shallow injections within the skin, whilst collimated jets typically resulted in deeper injections (Park et al., 2015). In contrast, the time duration of the jet injection and the volume of the drug that can be delivered inside the skin constitute some of the major differences between traditional jet injection technique (e.g., spring, compressed gas, voice coil etc.) and laser-induced jetting technique (Hogan et al., 2015; Cu et al., 2019; Miyazaki et al., 2019; Ruddy et al., 2019). Traditional jet injectors can deliver up to 1 ml of the drug either into muscular, subcutaneous, or dermal regions, whereas only a few micro-liters of drug can be injected to the intradermal tissue via microjet technique (Kiyama et al., 2019; Arora et al., 2007).

Baxter et al. showed that the penetration depth obtained by a liquid jet in hydrogel can be correlated with the jet power ($P_o = \frac{1}{8}\pi\rho D_j^2 v^3$) which depends on jet diameter (D_j) as well as jet speed (v) taken as the average velocity at the orifice (Schramm-Baxter and Mitragotri, 2004). Thus, one can deduce that the jet speed has a larger impact on the penetration depth in comparison to the jet diameter. In addition, jets with diameter more than 200 μm lead to higher possibility of pain and
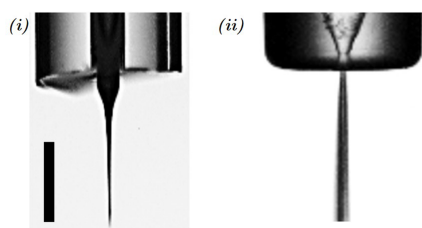
Fig. 1. Jet shape for (i) laser induced focused jet and (ii) dispersed jet from spring jet injector. Water was used as an injectate in both cases. Scale bar represents 2 mm.

bruising. Laser-induced jetting leads to jet diameters in the range of 50–100 µm. Thus, with a limited diameter range, a larger range of speeds is required to vary the power.

One study on laser-induced jets claims that microjets generated via laser focusing offer superior precision and less risk of tissue damage, which qualifies as a requirement of a needle-free jet injection technique (Delrot et al., 2018). As reported in a study by Römgens et al., high delivery efficiency up to 90% was achieved within the dermal layer with microjets (Römgens et al., 2016). As such, these low-dose microjets may be uniquely suited for intradermal drug delivery (Rodríguez et al., 2017). A potential remedy to circumvent low volume delivery is to operate in the repetitive pulse mode. Arora et al. reported successful delivery of sufficient dosage of insulin with minimum skin damage in rats by using low-volume microjets in repetitive mode (Arora et al., 2007) with piezoelectric actuation mechanism.

There has been no reported study to our knowledge on the effect of superheating of the liquid (i.e., possible damage to drug molecules) in laser-induced jet injections. To overcome this, different designs have been implemented in the past to generate liquid jets via laser pulse technique for application in needle-free injection. Rodríguez et al. (2017), Berrospe-Rodriguez et al. (2016) developed a microfluidic device to generate microjets by continuous wave laser technique. They were able to generate microjets with speed up to 29 m/s from a microchannel with a width of 250 µm. In another technique used by Han and Yoh (2010) and Han et al. (2011), a rubber layer absorbs the shock wave generated by the laser pulse to form a microjet of the drug contained in the adjacent chamber separated by the rubber layer. In these techniques, the pressure wave generated as a result of laser focusing is used to deflect or move the barrier, which forces the liquid stored in the adjacent chamber to move out as a jet. However, these techniques are not efficient (as measured by volume delivered into the skin from that expelled) and jet shapes are either not focused or have very low jet speeds, which may not be able to penetrate certain regions of skin.

Here, we have experimentally investigated the feasibility of laser-induced jetting for a combination of various parameters from the perspective of application in needle-free jet injections. Glycerol solutions with varying concentration (%w/w) were used to study the effect of viscosity. Other important parameters related to jet generation include incident laser pulse energy (E_i), capillary diameter (D_c), and distance of laser focusing point from the center of meniscus (L_F). The effect of these parameters was reflected on the jet speed, jet diameter, volume of the expelled liquid, and jet power. To translate the effect of these parameters for application in needle-free jet injections, we have conducted in vitro and ex vivo studies. Gelatin gel and porcine tissue were used as a proxy for human tissue. These skin models have similar mechanical properties as human tissues and have been used in the past due to the cost and unavailability of the human skin (Yoh and Jang, 2016; Tagawa et al., 2013; Kiyama et al., 2019; Miyazaki et al., 2019; Schramm-Baxter and Mitragotri, 2004). The mechanical properties of skin tissue vary with location, age, and other parameters. To mimic this variation in skin properties in an in vitro setting, we used various concentrations of gelatin hydrogel. While for ex vivo testing, we used porcine skin tissue. In both trials, the stand-off distance between the orifice and the

substrate was varied.

2. Materials and methods

2.1. Microjet generation

A schematic of the experimental setup is shown in Fig. 2(a), with the principal components being the pulsed laser, capillary, and high-speed camera. Heavy-walled glass capillary (*VitroCom, Mountain Lakes, NJ, USA*) with different inside diameter (D_c = 150 µm, 300 µm and 500 µm) and constant outside diameter of 3 mm was used. The glass capillary filled with liquid was connected to a syringe pump (*Legato 100, KD Scientific Inc., USA*) on one side and the other side was kept open to air. An energy meter (*ES111C, Thorlabs, Newton, NJ, USA*) placed behind the glass capillary, was used to measure the laser pulse energy.

A 532 nm, 6 ns, 120 mJ Nd:YAG laser (*Nano-S 120-20, Litron Lasers Ltd., UK*) was focused through a 20× microscope objective to a point inside the glass capillary filled with liquid. The incident laser pulse energy was varied by changing Q-switch delay. Glass capillaries cracked for incident laser pulse energy higher than 4.63±0.30 mJ (*Q-switch delay = 330 µs*) whereas E_i below 2.09 mJ (*Q-switch delay = 370 µs*) was insufficient for jet generation. Therefore, we used incident laser pulse energy in the range of 2.09±0.05 mJ to 3.94±0.21 mJ (*Q switch delay = 340 µs*). The distance of the laser focusing point from the center of the liquid meniscus, L_F was varied from 0.5 mm to 4 mm as defined in Fig. 2(b).
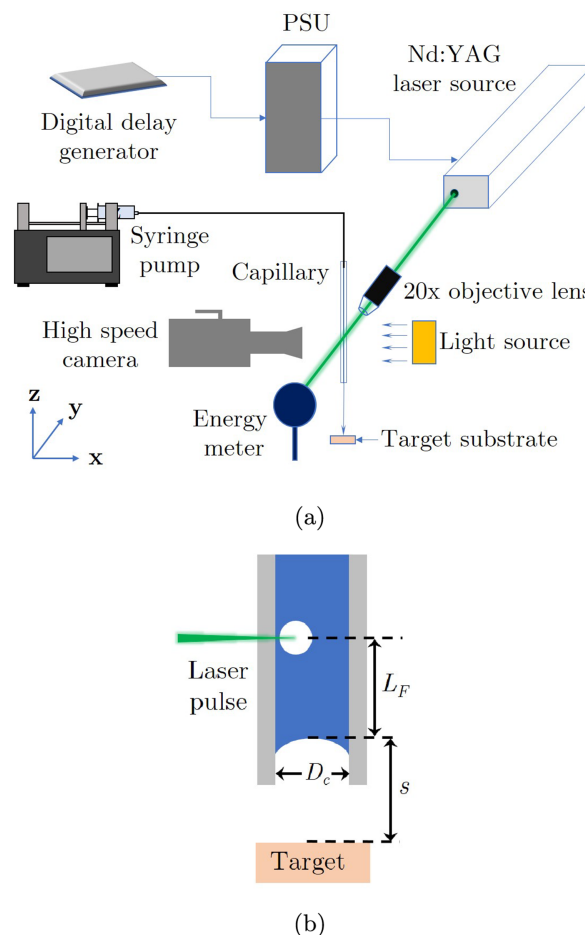

(a)

(b)

Fig. 2. Experimental setup. (a) Schematics and (b) parameters used in the study. (*Not to scale*).

2.2. Materials used

To conduct in vitro experiments, gelatin gel was prepared by mixing different concentrations (3%, 5%, and 8% w/w) of gelatin powder (*from Bovine skin – 225 g bloom, Type B, Sigma-Aldrich*) in Milli-Q water. Gelatin powder was mixed in water at 65 °C with constant stirring for 10 min. Gelatin solution was poured into the cuvettes and kept in a refrigerator at 4±1 °C for ~1 h. The cuvettes containing gelatin gel were taken out of the refrigerator and liquid jets were injected into the gel within an hour at room temperature conditions (*~ 21 °C, 60% Relative Humidity*). In addition to water, glycerol (*Macron*) solutions were prepared in two different concentrations (50% and 80% w/w in water as a solvent). Trypan Blue (*Sigma-Aldrich*) was used as a dye to aid visualization of the liquid jets injected into the gel and skin. Different stand-off distances, *s* (distance between the center of the liquid meniscus and the surface of the substrate to be injected) were used, ranging from 0.5 mm to 4 mm.

Porcine tissue procured from a local store, was used in ex vivo experiments for laser-induced jet injection. Dyed water was injected into the porcine tissue from different stand-off distances and focal lengths. After injection, porcine tissue was frozen to −4 °C. The frozen tissue was then cut to take cross-sectional pictures of the injection sites. Stand-off distance (*s*) and laser focusing distance (L_F) of 1 mm, 2 mm and 4 mm were used for injection in both gel and porcine tissue.

2.3. Imaging

A high-speed camera (*Phantom v1611, Vision Research Inc.*) was used to capture the jet generation at a frame rate of 10^5 frames per second, resolution of 1024×144, and an exposure time of 9 μs. A long-pass filter (*Mounted M30.5×0.5 Threaded – Red filter, Edmund Optics*), which allowed wavelengths >540 nm to the sensor, was used. Jet penetration and dispersion inside the gelatin gel was captured at a frame rate of 30,000 fps with resolution and exposure time of 896×400 and 9 μs respectively. The pixel size was in the range of 20–100 pixels per mm for capturing jet motion as well as the jet injection. Jet displacement and penetration of liquid inside the gelatin gel was tracked point by point using Photron FASTCAM Viewer software.

3. Results and discussion

3.1. Mechanism of jet generation via laser pulse

The jet is actuated by the absorption of optical energy from the laser pulse as follows: The concentration of energy from focusing results in optical breakdown (Padilla-Martinez et al., 2014; Rastopov and Sukhodolsky, 1991; Vogel et al., 1996), which releases a pressure impulse that deforms the concave meniscus (image (i) of Fig. 3a) of the liquid at the end of the capillary tube. This interaction results in the fast slender tip (image (ii) of Fig. 3a). The laser pulse causes rapid vaporization of the liquid that initiates the growth of a bubble; As this bubble grows (image (iii)), mass conservation dictates that the liquid ahead of the bubble is expelled from the open end of the tube. As such, the jet flow is sustained by the momentum of the jet tip and the expansion of the bubble behind it. Detailed explanations of the flow physics, backed by simulations can also be found elsewhere (Peters et al., 2013; Tagawa et al., 2013).

With typical scales $r \sim O(100)$ μm and $v \sim O(100)$ m/s, we find both Re, $We \sim O(10^4)$, showing that this is an inertia-dominated system at early times. The classical timescale $\tau = \sqrt{\rho r^3 / \sigma}$ for surface tension-driven breakup yields times of approximately 200–500 μs, which is of the correct order of magnitude for those seen in our experiments, however, we highlight the fact that the flow following the fast tip is subject to both viscous losses on the capillary wall, and suction pressure from collapse of the cavitation bubble, both of which decelerate the

liquid. In particular, the latter of these appears to be the principal mechanism that causes disturbance and irregular jet shape, which thus leaves the jet prone to early break-up. The cavitation bubble can also extend to the end of the capillary, which provides an inherent 'cut-off' point for the jet flow, limiting the available volume (V_a). As such, the expelled volume largely depends on the laser focal distance from the meniscus (L_f). For further reading on the breakup of jet emanating from laser-induced breakdown, we refer the reader to Refs. Padilla-Martinez et al. (2013) and Thoroddsen et al. (2009).

In this study, we have not used any specific adjuvants or lubricants which are generally used in the vaccines and affect the physical properties of the injectate. Moreover, the jets generated via laser focusing technique were not always axisymmetric due to high sensitivity to the location of the laser focusing point within the cross section of the capillary. Although not quantified, we observed that a slight variation in the laser focusing distance can affect the axial symmetry of the liquid jet.

3.2. Jet characterization

As discussed above, the interaction of the cavitation bubble with the capillary and jet flow renders an irregular jet shape, whose speed is difficult to define and measure. As such, we monitor the displacement of the tip of the jet with time to calculate the speed of the jet. Snapshots of the motion of the jet with time are shown in Fig. 3(a) for water with $L_F = 4$ mm and $E_i = 3.94$ mJ. The jet initially accelerates to reach maximum jet speed (v_{max}) after which we observe a slight but gradual deceleration over time until break-up. The initial acceleration can be attributed to flow focusing, whilst deceleration to factors such as air drag and jet thickening with time. It is important to note that differentiation of unsmoothed displacement data often results in noisy velocity plots (Vaughan, 1982; Craven and Wahba, 1978; Wood and Jennings, 1979), therefore we analyze our data for jet speeds using


(a)

(b)
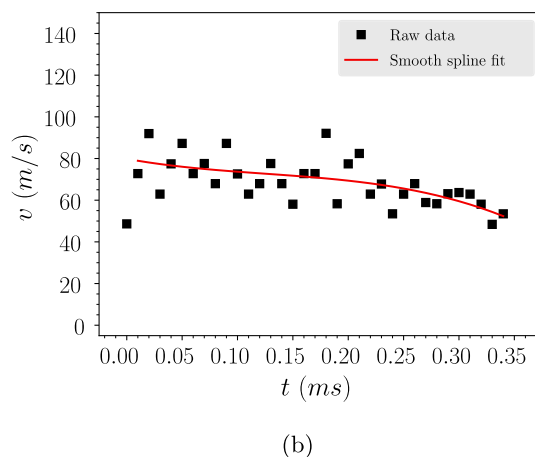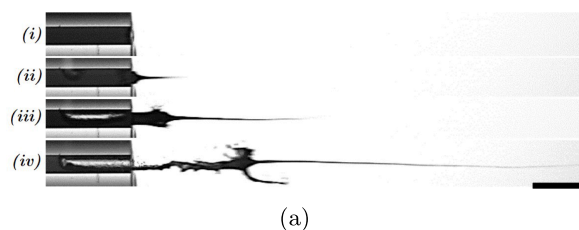
Fig. 3. Jet dynamics: (a) Snapshots of water jet generated with laser focused at $L_F = 4$ mm with incident laser pulse energy of $E_i = 3.94$ mJ for 500 μm capillary. Frames (i)–(iv) correspond to t = −10 μs, t = 20 μs, t = 70 μs and t = 200 μs, respectively. Scale bar represents 3 mm. (b) jet tip speed with time for the same realization as part (a).
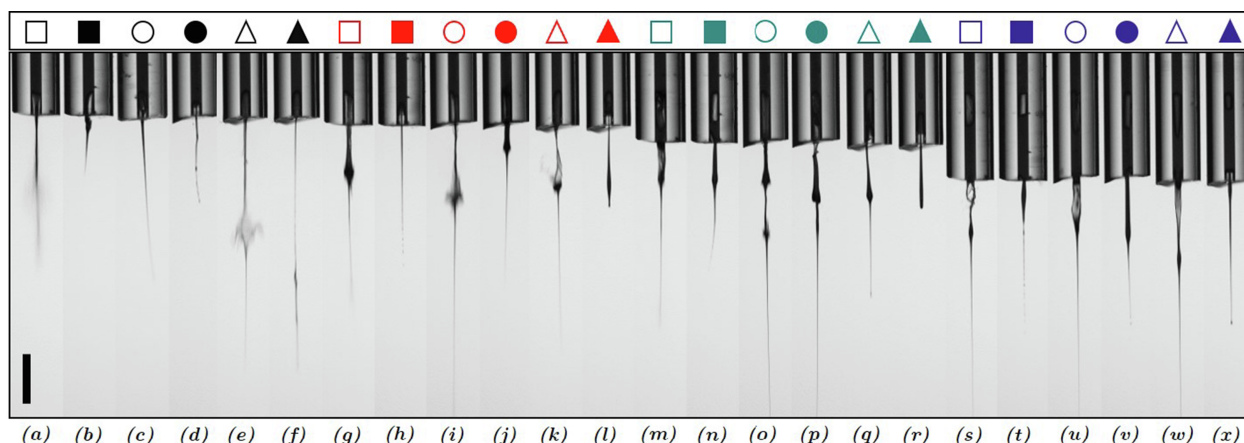
Fig. 4. Liquid jets of Water ($\square$), 50% glycerol ($\circ$) and 80% glycerol ($\triangle$) are used as empty and filled shapes to represent $E_i = 3.94$ mJ and $E_i = 2.09$ mJ respectively. Different colors represent different values of L_F (0.5 mm, 1 mm, 2 mm and 4 mm). Snapshots of liquid jet corresponds to: (a) t = 45.45 μs, (b) t = 91 μs, (c) t = 0.22 ms, (d) t = 0.22 ms, (e) t = 91 μs, (f) t = 0.22 ms, (g) t = 91 μs, (h) t = 0.36 ms, (i) t = 91 μs, (j) t = 45.45 μs, (k) t = 91 μs, (l) t = 0.22 ms, (m) t = 45.45 μs, (n) t = 0.22 ms, (o) t = 91 μs, (p) t = 0.22 ms, (q) t = 0.22 ms, (r) t = 0.36 ms, (s) t = 91 μs, (t) t = 0.36 ms, (u) t = 91 μs, (v) t = 0.36 ms, (w) t = 91 μs and (x) t = 0.36 μs. Scale bar represents 3 mm. (For interpretation of the references to colour in this figure legend, the reader is referred to the web version of this article.)

cubic spline fitting as shown in Fig. 3(b). A spline fitted with the raw velocity-time data to show the jet speed with time is presented in Fig. 3(b). The jet tip develops into a highly focused shape at a distance of 1 mm to 2 mm from the meniscus, which is also used as a typical stand-off distance. As such, we use the velocity at this point for the impact speed, i.e., $v_i \equiv v_j(x = 2$ mm), which was used along with maximum jet speed for jet characterization unless otherwise specified.

Whilst a typical jet shape consists of a highly focused, thin jet ($d \approx 50$ μm) followed by a slower, thicker portion ($d \approx D_o$), there is variation depending upon the exact configuration of parameters used. In essence, higher viscosity leads to jets with thicker tips, yet there is substantial interaction with the other parameters.To highlight this, a montage of jets is presented in Fig. 4. Spray type jet (e.g., Fig. 4(a, e)) was obtained for smaller L_F with higher E_i followed by collimated stream of liquid jet. In contrast, more slender, stable jets were observed for water, 50% glycerol and 80% glycerol solution at higher $L_F \geqslant 1$ mm depending on the magnitude of laser pulse energy e.g. Figs. 4($g - k$, m, o, p, $s - w$). One can notice from the snapshots presented in Fig. 4 that 50% glycerol showed longer focused jets with stable cross section in comparison to water and 80% glycerol solution. In case of low E_i, jet tip of 80% glycerol solution was observed to have round shape with laser focused farther away (4 mm) from liquid meniscus. Fig. 5 shows the diameter of the jet at a constant distance of 2 mm from the meniscus with time. Jet tip diameter of the highly
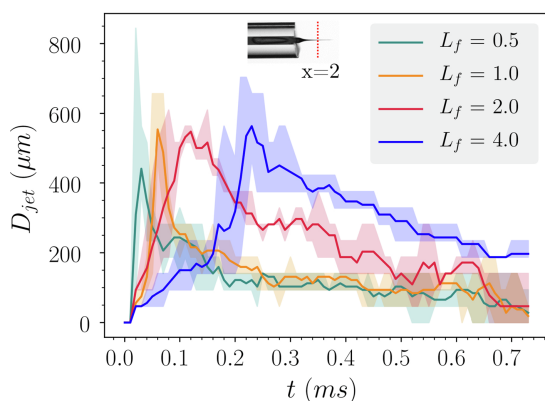
focused part of the jet generally lied in the range of $\sim$30–100 μm. One can observe that the thicker portion of the jet is typically 400–850 μm in diameter but depends on the focal distance, L_f, as observed in Fig. 5. To understand the effect of dye, jets were generated with both transparent water and with dyed water. Fig. S8 shows that the jet speed was higher for dyed water in comparison to the transparent water as adding dye to water increased its absorbed laser energy.
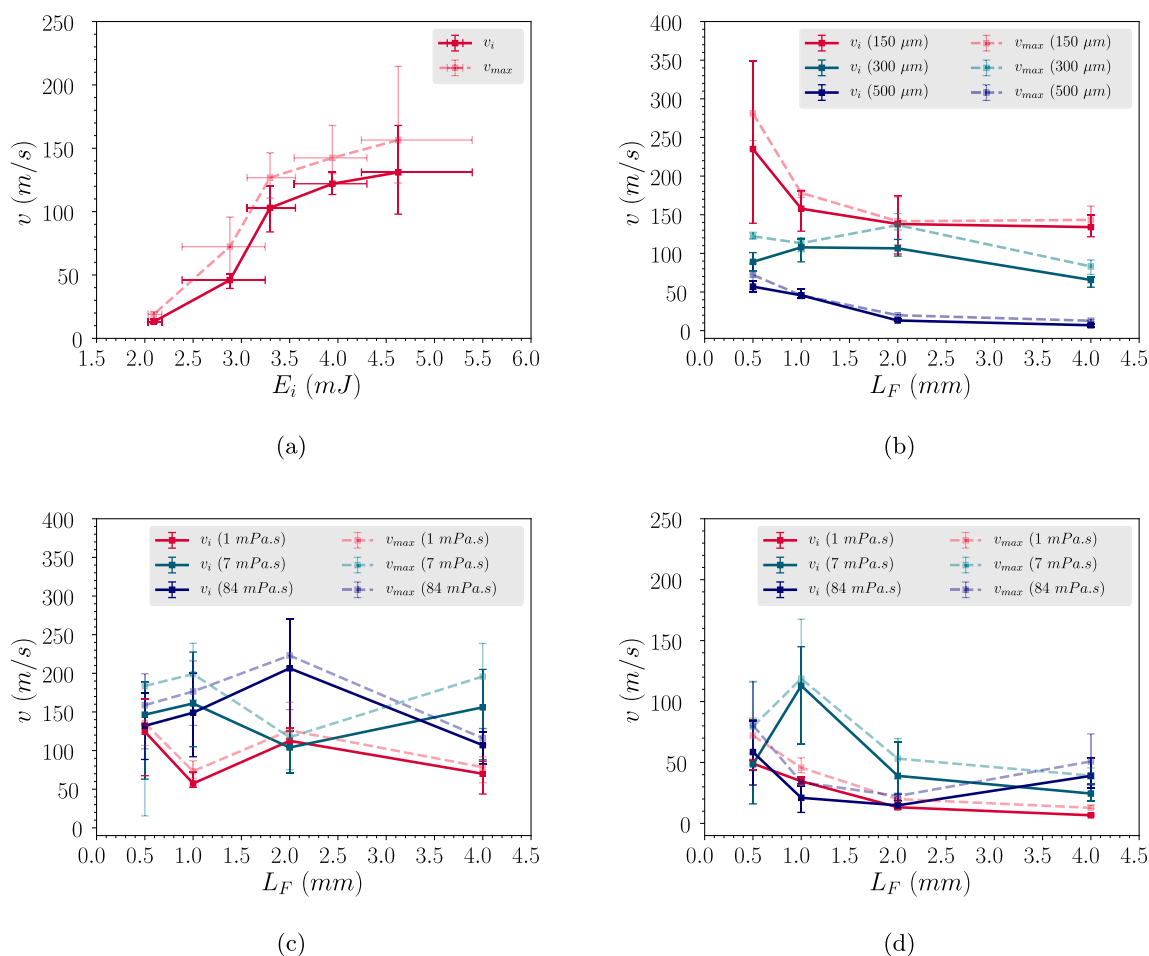
3.3. Effect of incident laser pulse energy

Incident laser pulse energy was varied from 2.09 mJ to 4.63 mJ to generate microjets from water when focused inside a 500 μm glass capillary for a constant L_F. Variation in jet speed at impact and maximum jet speed with incident laser pulse energy is presented in Fig. 6(a). We observe that the jet speeds increase monotonically with laser pulse energy, albeit in a nonlinear fashion. We also observe more intrasample variation at $E_i = 4.63$ mJ since this energy is close to the threshold of capillary damage. Nonetheless, this data shows that the jet speed can be fine-tuned from $\mathcal{O}(10)$-$\mathcal{O}(100)$ m/s by variation of pulse energy alone. One important point not considered herein is the effect of localized heating on the physicochemical properties of the liquids, since higher energy implies higher propensity for damage to sensitive molecules, which needs to be addressed in future research efforts. From a statistical standpoint, the effect of E_i was significant for both impact jet speed ($p \ll 0.05$) and maximum jet speed ($p \ll 0.05$).

3.4. Effect of laser focusing point and capillary diameter

The laser focal point relative to the meniscus, L_f dictates how much volume is available to be ejected from the open side of the capillary, whilst the magnitude of the pressure wave generated by laser focusing diminishes as L_f increases. As such, it is instructive to examine the effect of L_f on jet speed, which is shown in Fig. 6(b) for various capillary diameters ($D_c = 150$ μm, 300 μm and 500 μm) for $E_i = 2.09$ mJ.

For 150 μm capillary, maximum jet speed reached as high ($\sim$350 m/s) as speed of sound in air for $L_F = 0.5$ mm. For $D_c = 300$ μm, the jet speeds remained relatively constant at $\sim$ 100 m/s, whilst for $D_c = 500$ μm, we observed a decrease from $\sim$ 50 $\rightarrow$ $\sim$ 10 m/s. There is a high possibility that liquid jets with such low speeds would not be able to penetrate skin and deliver the liquid within the skin. Here, one should note that the incident pulse energy used is 2.09 mJ, whereas higher pulse laser energy as high as 3.94 mJ gives typical jet speed of $\sim$150 m/s, which we have used for in vitro and ex vivo studies.

Fig. 5. The diameter of the laser induced jet (measured at x = 2 mm from orifice) with time for different laser focusing distances ($E_i = 3.94$ mJ). Inset shows a laser induced jet expelled out of a glass capillary with a dashed line corresponding to x = 2 mm.

Fig. 6. Jet speed for (a) water focused with laser with different impulse laser energy (E_i) for L_F = 2 mm, (b) water focused at different L_F for E_i = 2.09 mJ, (c) water focused with laser for capillaries with different L_F for E_i = 3.94 mJ and (d) different liquids inside 500 μm capillary for different L_F with E_i = 2.09 mJ.

A near linear increase in characteristic jet speeds (v_i and v_{max}) was observed for decreasing capillary inside diameter from 500 μm to 150 μm. Therefore, the combined effect of small D_c and higher E_i results in high-speed focused jets. Two-way ANOVA analysis showed that jet impact speed and maximum jet speed were significantly affected by L_F ($p < 0.05$) and D_c ($p < 0.05$) without any evidence of any interaction effect of these parameters ($p > 0.05$). The only drawback of these high-speed jets is low volume ejected. Thus, the selection of parameters largely depends on the compromise of the jet speed and the volume requirements.

3.5. Effect of liquid viscosity

Glycerol solutions with different concentrations were used to study the effect of liquid viscosity on the jet generation via laser focusing. For E_i = 3.94 mJ and L_f = 0.5–4 mm, the effect of viscosity was studied by using glycerol concentrations 0% (water), 50% and 80%, with the corresponding jet speeds presented in Fig. 6(d). Laser-induced jetting for different glycerol solutions for L_F = 1 mm and E_i = 3.94 mJ are available as supplementary videos S1–S3.

For E_i = 3.94 mJ, the effect of liquid viscosity on jet speed with an interplay of laser focusing distance is shown in Fig. 6(c). For water, impact jet speed and maximum jet speed for L_F = 1 mm were relatively low. Jets were faster for 50% and 80% glycerol solutions for L_F = 1 mm. Interestingly, abnormal behavior in terms of characteristic jet speeds was showed at different L_F by the liquids used. One can notice that the kink in jet speeds for 50% glycerol and 80% glycerol solutions was observed for L_F = 2 mm, where jet speed increased for 80%

glycerol solution and decreased for 50% glycerol solution. Overall, the effect of μ was significant on v_i ($p < 0.05$) with the insignificant effect of L_F ($p > 0.05$). Whereas, μ and L_F both showed significant effect on v_{max} ($p < 0.05$) with mildly significant effect of interaction ($p < 0.05$) among the viscosity and laser focusing distance.

For E_i = 2.09 mJ and L_f = 0.5 mm, jet speeds were in a range of ~50–80 m/s for different liquids used. For L_F = 1 mm and 2 mm, jets generated with 50% glycerol solution were faster than water jets followed by 80% glycerol solution. The maximum jet speed ($v_j \approx$ 120 m/s) for this parameter range occurred for L_f = 1 mm with 50% glycerol. This interesting result may represent a trade-off between viscous effects and enhanced laser absorption/thermocavitation process due to the glycerol molecules, but as yet is not fully understood. At a farther laser focusing distance of 4 mm, 80% glycerol solution showed higher jet speeds in comparison to water and 50% glycerol solution. Here, the effect of L_F was significant on v_i ($p < 0.05$) with the insignificant effect of μ ($p > 0.05$). Whereas, μ and L_F, both showed significant effect on v_{max} ($p < 0.05$) without any significant effect of interaction ($p < 0.05$) among the viscosity and laser focusing distance.

3.6. Volume ejected

The percentage delivery by volume is an important factor which dictates the effectiveness of any drug delivery technique. Here, when the laser is focused inside the capillary filled with any liquid, liquid volume from the focusing point to the liquid meniscus open to air is free or available volume which can be expelled depending on the magnitude of incident laser energy. The volume expelled was estimated using

(a)

(b)

(c)
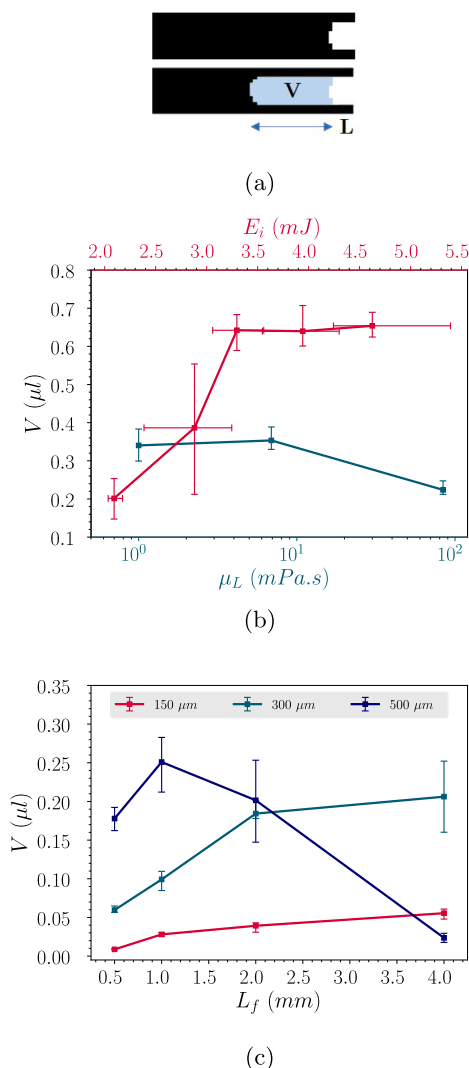
Fig. 7. Estimation of liquid volume expelled. (a) background subtraction of frames showing liquid level inside the capillary, (b) variation of expelled volume with incident laser energy (L_F = 2 mm, Dyed water) and liquid viscosity (L_F = 1 mm, E_i = 3.94 mJ) for a glass capillary with D_c = 500 μm and (c) effect of D_c and L_F on expelled liquid volume for E_i = 2.09 mJ.

background subtraction with a custom Matlab script. Fig. 7(a) shows two frames before and after the jet has been expelled with shaded part indicating expelled liquid. The length of liquid plug, L (not to be confused with L_F) was used in the estimation of the expelled liquid volume using $V = \frac{1}{4}\pi D_c^2 L$, where D_c is the inside diameter of the capillary.

The effect of liquid viscosity on the volume expelled is presented in Fig. 7(b) for L_F = 1 mm and a glass capillary with D_c = 500 μm. Volume expelled for water and 50% glycerol was nearly the same for E_i = 3.94 mJ and L_F = 1 mm. However, 80% glycerol showed lower volume ejection with lower jet speed in comparison to dyed water due to viscous effects and different absorption limits of laser energy. Fig. 7(b) also shows effect of incident laser energy on volume of the liquid expelled for laser focusing distance of 2 mm inside a capillary with D_c = 500 μm. The initial volume of the liquid expelled increased with the increase in magnitude of laser energy. After $E_i \simeq 3.3$ mJ, nearly the same volume was expelled, showing the maximum limit of the expelled volume for the range of laser energy used. The effect of both parameters (μ ($p < 0.05$) and E_i ($p < 0.05$)) was significant on the volume of the liquid expelled.

Fig. 7(c) shows volume of the liquid expelled with variation in D_c and L_F for E_i = 2.09 mJ. It is noteworthy that with increase in L_F,

larger volume is available for expulsion. However, more force is required to push the liquid column in the form of a liquid jet, which requires more laser energy. Here, the laser energy was kept constant to focus on the effect of variation in L_F on the V. For 150 μm capillary, the expelled volume increased as the laser focusing point was moved farther from the liquid meniscus. Similarly, the expelled volume was higher for larger L_F for 300 μm capillary. In case of 500 μm capillary, the volume expelled decreased after the initial increase in L_F from 0.5 mm to 1 mm. For $L_F > 1$ mm, laser energy was not sufficient to expel the larger available volume, resulting in a sharp decrease in volume ejected. Only ~2–3% of the available volume was expelled for L_F = 4 mm from 500 μm capillary. Two-way ANOVA analysis showed that the effects of L_F ($p < 0.05$) and D_c ($p < 0.05$) were significant, but also their interaction ($p < 0.05$). This means that regardless of other settings, changing the focal length or the capillary diameter will change the expelled volume, but that the magnitude of change will depend on the other.

3.7. In vitro studies

To check the feasibility of microjets generated via laser focusing in needle-free jet injections, we conducted microjet injections inside the gelatin gel. Due to the high cost and unavailability of human skin, substitute hydrogels with a range of mechanical properties were used to understand the penetration and dispersion of the liquids. Human dermal tissue is an intricate structure of fibers (Graham et al., 2019) with varying mechanical properties depending on the location of the skin, aging, loading and other effects (Escoffier et al., 1989; Hagisawa and Shimada, 2005; Sangeorzan et al., 1989). However, homogeneous hydrogels only capture the stiffness of the human tissue without any large variation in mechanical properties within the matrix. Mechanical properties of the gelatin gel with three different concentrations used here, have been reported in our previous study (Rohilla and Marston, 2019).

Gelatin gel was prepared in three different concentrations ($3\%_{w/w}$, $5\%_{w/w}$, and $8\%_{w/w}$) corresponding to varying mechanical strength. Higher laser pulse energy of 3.94 mJ was used to generate high speed microjets for injection in the gelatin gel. Stand-off distance between the meniscus and the target is an important parameter in jet injection (Rohilla and Marston, 2019) and therefore we investigated a range of stand-offs from s = 1–4 mm with fluid viscosity in the range of 1–85 mPa.s.

3.8. Penetration dynamics

A high-speed focused jet actuated by the laser pulse impinged on the surface of the gelatin gel. High inertial force creates a hole which aids liquid jet propagation inside the gel. Snapshots showing penetration dynamics of water jet inside $5\%_{w/w}$ gelatin gel for a stand-off distance of 2 mm are presented in Fig. 8(a). The incoming liquid continues to propagate inside the gel until the elastic relaxation forces overcome the inertial forces. At this point, liquid propagation and dispersion reaches a maximum, as shown in frame at time, t = 0.67 ms. Penetration depth at this stage is denoted as $d_{p,max}$. After this stage, the dispersion pattern shrinks due to elastic relaxation forces and some of the deposited liquid escapes the gel. Final penetration depth ($d_{p,f}$) after complete relaxation (t = 12 ms in Fig. 8(a) was used to characterize the jet injection performance into the gel (and porcine tissue model in ex vivo studies). Supplementary Fig. S4 shows transient jet dynamics for variation in different parameters. Supplementary video S4 shows laser-induced jet injection of water into $5\%_{w/w}$ gelatin gel for s = 1 mm, L_F = 4 mm and E_i = 3.94 mJ.

3.9. Penetration depth

Penetration depth after the jet injection followed by the relaxation
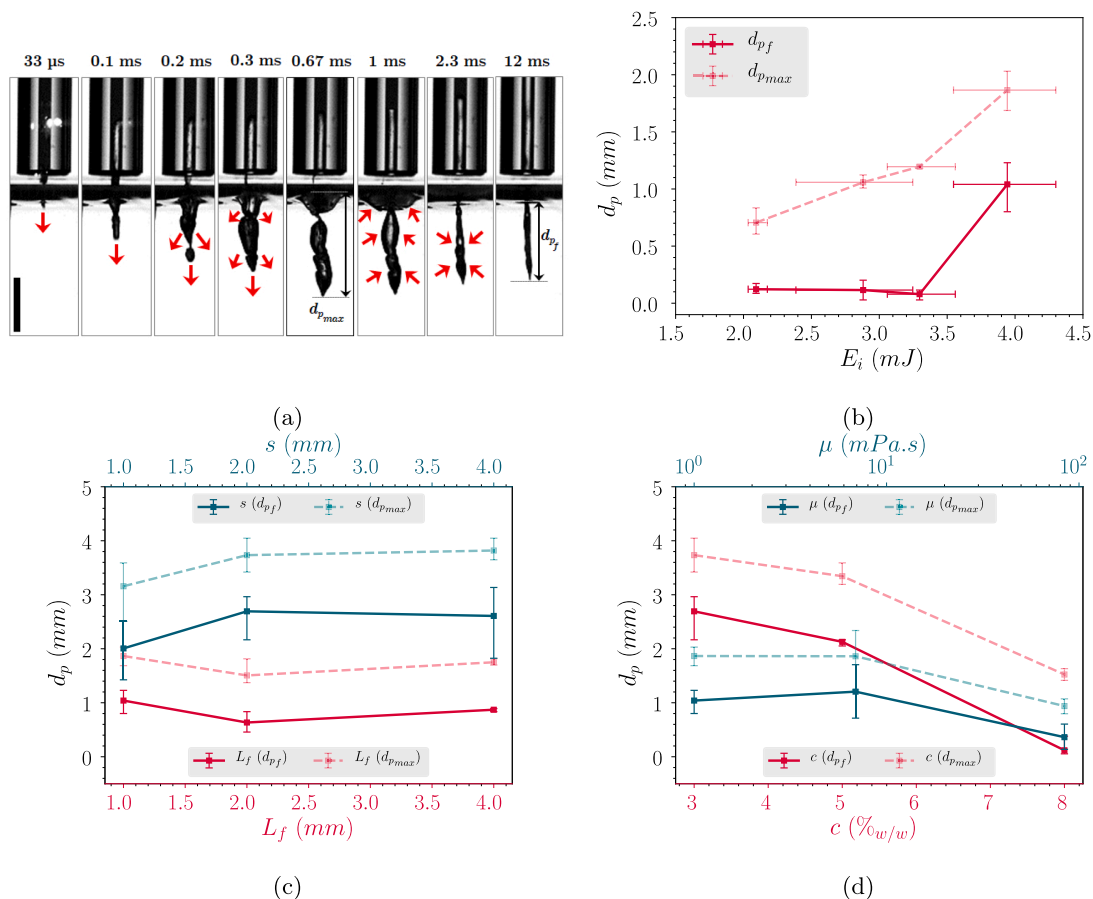
Fig. 8. Effect of different parameters on the penetration depth (d_p) in proxy gel. (a) snapshots of transient penetration dynamics of water jet into 5%$_{w/w}$ gelatin gel for $L_F = 4$ mm and $s = 2$ mm (Scale bar: 3 mm), (b) effect of incident laser pulse energy (E_i) on d_p for 5 %$_{w/w}$ gelatin gel ($L_F = 1$ mm, $s = 2$ mm), (c) effect of s on d_p for 3%$_{w/w}$ gelatin gel with $L_F = 2$ mm and effect of L_F on d_p for 5%$_{w/w}$ gelatin gel with $s = 2$ mm, (d) effect of gel concentration and liquid viscosity (μ_L) on d_p. n = 4.

($d_{p,f}$) and maximum penetration depth during jet injection ($d_{p,max}$) were used to compare the performance of jet injection with variation in parameters including stand-off distance (s), concentration of the gelatin gel (c in %$_{w/w}$), viscosity of the liquid injected (μ), laser pulse energy (E_i) and distance of laser focusing point from the center of the meniscus.

In case of increasing laser energy, penetration depth was nearly the same for E_i up to ~3.30 mJ as shown in Fig. 8(b). At $E_i = 3.94$ mJ, water penetrates deeper inside the gelatin gel. Due to high jet speed at impact for $E_i = 3.94$ mJ, impact jet power was also higher than that for other magnitudes of laser energy. Overall, the effect of incident laser pulse energy was highly significant for both the maximum penetration depth ($p \ll 0.05$) and the final penetration depth ($p \ll 0.05$).

Jet focusing does not occur at the meniscus and needs some distance to develop. Thus, stand-off distance is an important parameter which affects the drug delivery via laser-induced jets. Fig. 8(c) shows that with smaller stand-off distance the liquid jet reached lower penetration depth as compared to larger stand-off distance of 2 mm and 4 mm. For the stand-off distance of 2 mm and 4 mm, the penetration depth inside the gel was nearly the same. Also, increasing the stand-off distance can compromise the precision in delivering the drug at a specific site. Thus, a distance of 2 mm between the substrate and the liquid meniscus is recommended to deliver the liquid to a larger penetration depth without compromising the precision of the drug delivery. The liquid microjets obtained for $L_F = 0.5$ mm have low volume and do not form a stable jet. Thus, the distance of the laser focusing point from the meniscus was varied from 1 mm to 4 mm to understand the effect of L_F on d_p. As can be seen from the Fig. 8(c) by varying L_F, the final penetration depth ranged from ~0.5 mm to ~1.2 mm inside the gel. The maximum

penetration depths inside the gel were higher (ranging from ~1.4 mm to ~2 mm). Statistically, the effect of L_F was significant on both $d_{p,f}$ ($p < 0.05$) and $d_{p,max}$ ($p < 0.05$).

As discussed earlier, the behavior of variation in mechanical properties of skin tissue can be achieved by varying gelatin concentration. Liquid jet achieves larger penetration depth inside the softest gel with low concentration of gelatin. With increase in the gel concentration, depth up to which jet can penetrate decreases as can be seen in Fig. 8(d). For shallow penetration depth like in 8% gelatin gel, most of the liquid is rejected on the surface as splashback due to strong elastic forces of the high concentration gelatin gel. Overall, the effect of gel concentration was highly significant for both the maximum penetration depth ($p \ll 0.05$) and the final penetration depth ($p \ll 0.05$).

Fig. 8(d) also shows the effect of viscosity of the liquid to be injected inside the 5% gelatin gel for laser focused at a distance of 1 mm from the meniscus at an incident laser energy of 3.94 mJ. The impact jet power (P_i) is another parameter which plays an important role to relate the penetration depth achieved by a liquid jet for specific jet parameters. Assuming constant jet tip speed and using jet tip diameter at impact (using $s = 2$ mm), the impact jet power was estimated for different parameters and is presented in Fig. 9. The final penetration depth was higher for 50% glycerol solution followed by water and 80% glycerol solution. Due to the higher impact speed, 50% glycerol solution has the highest impact jet power, followed by 80% glycerol solution and water as $P_i \propto v_i^3$. However, the penetration depth does not follow the order of impact jet power, which means jet power cannot dictate the penetration depth alone and the jet shape and duration of the jet ejection are crucial factors to be considered to understand to estimate the final penetration depth. Statistical analysis shows that the viscosity
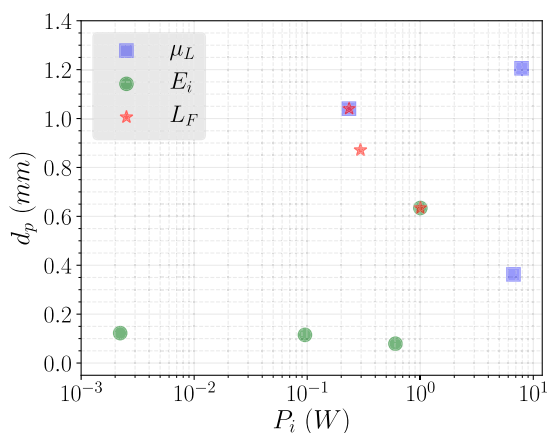
Fig. 9. Penetration depth as a function of the jet power at impact (x = 2 mm). Magnitude of jet power was varied by varying μ_L, E_i and L_F (*as shown in legends*).

effects are significant for both maximum penetration depth ($p < 0.05$) and final penetration depth ($p < 0.05$).

Apart from the penetration depth, we also studied the effect of various parameters on the lateral dimension (width) of the dispersion pattern. Figs. S5 and S6 in supplementary info show the effect of these parameters on the width and the depth of the dispersion pattern. The percentage shrinking of the dimensions of the dispersion pattern due to the elastic relaxation for various parameters is presented in Fig. S7. As one can notice, the shrinking of the patterns either in terms of the width or the depth depends on the different parameters. The dispersion patterns shrunk in the range of ~40% to ~90% in either dimension due to the elastic relaxation.

3.10. Ex-vivo studies

Ex vivo studies of laser-induced jet injections were conducted on porcine tissue as a model for human skin. A capillary diameter of 500 µm was used for all trials with different stand-off distances and different laser focusing distances. However, the laser pulse energy was kept constant at ~3.94 mJ, which is the maximum possible without breaking the capillary. Porcine tissue with a fat layer on top was injected with the dyed water (Fig. 10(a)). After injection, tissue was frozen and medially sectioned to visualize the injection site. The injected fluid formed blebs whose cross-sectional view is presented as an inset in Fig. 10(a) showing the bleb width (w) and the depth (h). These dimensions were used to characterize the liquid dispersion inside the skin.

Snapshots of the water jet injection for L_F = 4 mm are shown in Fig. 10(b). The impinging jet creates a hole and propagates into the skin. However, the width of the jet was not constant, as the thicker portion of the jet usually follows the thin tip of the jet. Thus, as the jet gains width, further propagation of the liquid jet slows down. As the thicker portion is larger than the hole created by the focused part, the liquid gets rejected as splashback. The red outline at t = 0.4 ms shows the splashback of the liquid rejection on the surface of the skin. Thus, laser-induced jets primarily deliver liquid via the focused part, whereas the thicker part of the jet is largely rejected due to a confluence of the narrow hole formed by the focused jet and the slower jet speed. Splashback of liquid is undesirable resulting in lower delivery efficiency and contamination.

The dimensions of the bleb (bleb depth, h and bleb width, w) formed as a result of the jet injection are plotted in Fig. 10(c). One can observe that the blebs formed within the tissue were relatively larger in width as compared to the depth of the bleb (i.e., $h < w$) for different combinations of L_F and s. Aspect ratio of the blebs ($AR = h/w$) was used a parameter to represent the bleb dimension; $AR > 1$ implies an elongated dispersion pattern in the direction of the jet, whereas $AR < 1$

indicates an oblate bleb shape which is more desirable for intradermal injections targeting immune cells therein. Fig. 10(d) shows the effect of s and L_F on AR. Bleb dimensions were in nearly similar range for variation in s and L_F except for the case of s = 4 mm and L_F = 2 mm, where the depth of the bleb formed in the skin was relatively larger than the width (i.e. aspect ratio of the bleb was relatively higher). Diffusion of the liquid from the surface could also be a contributing factor in the wide shape of the blebs. Two-way ANOVA analysis showed no significant effect of laser focusing point ($p > 0.05$), stand-off ($p > 0.05$) nor any interaction between these parameters ($p > 0.05$) on aspect ratio of the blebs. The percentage delivery inside the skin varied from ~5% to ~30% as can be observed from Fig. 10(e), which means a larger amount of the liquid expelled as a jet was rejected in the form of the splashback. The depth of the bleb within ~2 mm and a reasonable percentage delivery shows good feasibility of the laser-induced jet technique in intradermal injection. However, the occurrence of splashback must be controlled (Hogan et al., 2015; Canter et al., 1990) to minimize product wastage and contamination possibly via the reduced or zero stand-off distance, as well as pre-tensioning skin (Cappello et al., 2019). Laser-induced jet injection of water into porcine skin is shown in supplementary video S5 (s = 2 mm, L_F = 4 mm and E_i = 3.94 mJ).

3.11. Cavitation effect after the jet injection

Since the maximum volume deliverable from a single laser pulse is very limited (<0.9 µL). several attempts have been made to exploit the ability of pulsed lasers to deliver multiple doses and thus, by accumulation, deliver a more substantial volume. This has been referred to as the 'repetitive microjet regime' (Cu et al., 2019; Arora et al., 2007; Römgens et al., 2016; Krizek et al., 2020; Loreto Oyarte Gálvez et al., 2019) and, whilst a detailed examination is out of the scope of the current study we demonstrate what happens after a single microjet ejection within the liquid contained in the capillary. As shown in Fig. 11, the cavitation bubble stays within the liquid even after the jet has been expelled. Fig. 11*a-d*) shows bubble dynamics with time. In the last frame (d), nearly the entire injection has been ejected and the bubble stays back. Laser focusing at the same point or near this point during repetitive laser focusing generate nonuniform jets and could also damage the capillary. Figs. S12–S14 shows several cases where the cavitation bubble stays within the liquid even after the end of the jet ejection process. This phenomenon depends on the laser energy and the distance of the laser focusing point from the meniscus for a given capillary as shown in the supplementary figures. In other cases, where no cavitation bubble was observed after single jet ejection, liquid meniscus can be maintained at a specified level using a syringe pump to deliver consistent repetitive injections.

4. Conclusions and outlook

To summarize, we have studied the effect of various parameters related to laser-induced microjets, including the laser focal point, pulse energy, capillary diameter and liquid viscosity, all of which showed significant effects on the speed of the resulting microjets. These jets (with diameters below 100 µm) were capable of penetrating both gelatin substrates and ex vivo tissue samples, albeit with low efficiency (<30%) due to splashback.

In gelatin targets, the injections result in narrow channel-like formations with typical depths of 1–4 mm, whereas porcine tissue exhibited shallow and wider injections, with depths typically less than 1 mm. The latter may be preferable for the purposes of targeting immune cells in the intradermal tissue, and therefore renders microjet techniques viable for intradermal injections.

From an applications perspective, the technique is attractive for rendering exclusively intradermal injections which can minimize pain and improve patient compliance. Yet the low volume of the technique

(a)

(b)

(c)

(d)

(e)
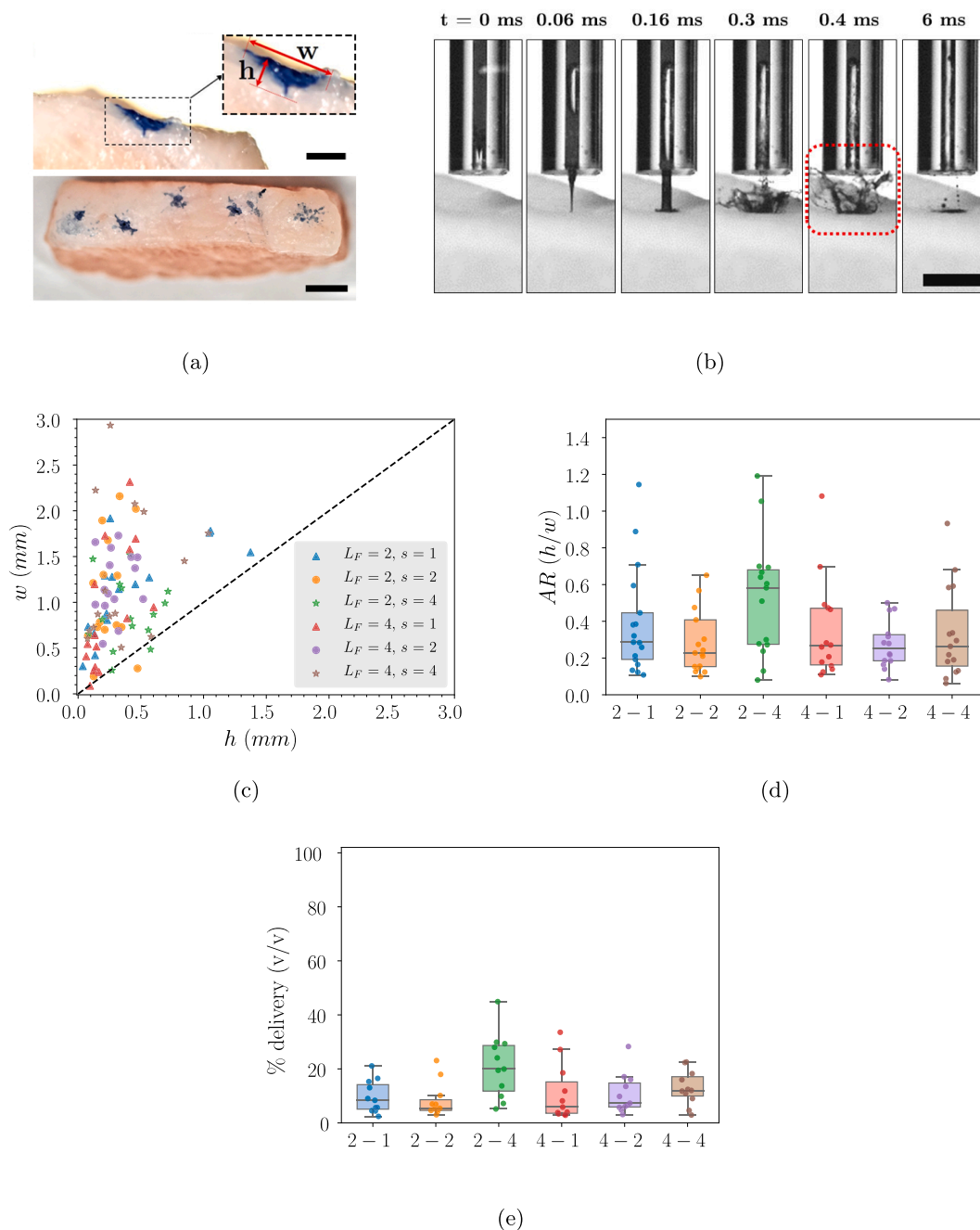
Fig. 10. Ex-vivo studies (a) cross-sectional and top view of the porcine tissue after 5 injections via jets generated via laser focusing Scale bars in upper and lower sections represents 2 mm and 5 mm respectively. (b) snapshots of dyed water injection into the porcine tissue from the glass capillary with inside diameter of 500 μm with L_F = 4 mm, s = 2 mm and E_i = 3.94 mJ. Scale bar represents 3 mm. (c) Comparison of width (w) and depth (h) of the blebs formed within the skin after the injection, (d) dimensions of the bleb formed within the porcine tissue after water injection via laser induced jetting for different L_F and s. (e) percentage delivery of the liquid injected inside the skin from the total expelled volume for different L_F and s. X-axis ticks in *(d)* and *(e)* represents $L_F - s$, e.g. $2 - 1$ means L_F = 2 mm and s = 1 mm.

(< 0.9 μL in our present work) and lower efficiency will make it difficult to develop into a wide-spread commercially viable option. In addition, one must consider the state of the skin rendered by location on the body, patient age, and hydration. However, novel systems that do not require large high-power pulsed lasers may provide a path forward toward commercialization but must first address the issue of injection efficiency and handling of both low-and high-viscosity fluids.

CRediT authorship contribution statement

Pankaj Rohilla: Data curation, Formal analysis, Writing - original draft. **Jeremy Marston:** Conceptualization, Writing - review & editing, Supervision.

Declaration of Competing Interest

The authors declare that they have no known competing financial interests or personal relationships that could have appeared to
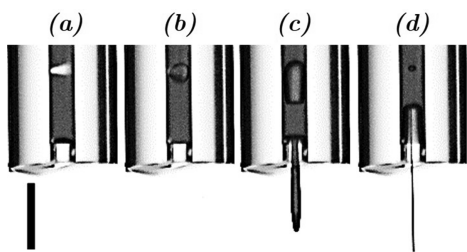
Fig. 11. Cavitation bubbles left after liquid expelled as a jet for 80% glycerol as liquid with laser focused at L_F = 2 mm with E_i = 2.0 mJ. Snapshots corresponds to: (a) t = 0 ms, (b) t = 0.055 ms, (c) 0.28 ms and (d) t = 2.22 ms. Scale bar represents 2 mm.

influence the work reported in this paper.

Acknowledgments

Appendix A. Supplementary material

Supplementary data associated with this article can be found, in the online version, at https://doi.org/10.1016/j.ijpharm.2020.119714.

References

Arora, Anubhav, Hakim, Itzhak, Baxter, Joy, Rathnasingham, Ruben, Srinivasan, Ravi, Fletcher, Daniel A., Mitragotri, Samir, 2007. Needle-free delivery of macromolecules across the skin by nanoliter-volume pulsed microjets. Proc. Natl. Acad. Sci. 104(11), 4255–4260.

Berrospe-Rodriguez, Carla, Visser, Claas Willem, Schlautmann, Stefan, Ramos-Garcia, Ruben, Rivas, David Fernandez, 2016. Continuous-wave laser generated jets for needle free applications. Biomicrofluidics 10 (1), 014104.

Brennen, Christopher E., 2014. Cavitation and Bubble Dynamics. Cambridge University Press.

Canter, Jeffrey, Mackey, Katherine, Good, Loraine S., Roberto, Ronald R., Chin, James, Bond, Walter W., Alter, Miriam J., Horan, John M., 1990. An outbreak of hepatitis b associated with jet injections in a weight reduction clinic. Arch. Internal Med. 150 (9), 1923–1927.

Cappello, Chris, Wixey, Matt, Bingham, John W., 2019. Needle-free intradermal injection device, June 18 2019. US Patent 10,322,238.

Craven, Peter, Wahba, Grace, 1978. Smoothing noisy data with spline functions. Numerische mathematik 31 (4), 377–403.

Cu, Katharina, Bansal, Ruchi, Mitragotri, Samir, Rivas, David Fernandez, 2019. Delivery strategies for skin: comparison of nanoliter jets, needles and topical solutions. Ann. Biomed. Eng. 1–12.

Delrot, Paul, Hauser, Sylvain P., Krizek, Jan, Moser, Christophe, 2018. Depth-controlled laser-induced jet injection for direct three-dimensional liquid delivery. Appl. Phys. A 124 (9), 616.

Escoffier, Catherine, de Rigal, Jean, Rochefort, Annie, Vasselet, Régis, Lévêque, Jean-Luc, Agache, Pierre G., 1989. Age-related mechanical properties of human skin: an in vivo study. J. Investig. Dermatol. 93(3).

Gálvez, Loreto Oyarte, Pérez, Maria Brió, Rivas, David Fernández, 2019. High speed imaging of solid needle and liquid micro-jet injections. J. Appl. Phys. 125 (14), 144504.

Graham, Helen K., Eckersley, Alexander, Ozols, Matiss, Mellody, Kieran T., Sherratt, Michael J., 2019. Human skin: composition, structure and visualisation methods. In: Skin Biophysics. Springer, pp. 1–18.

Hagisawa, Satsue, Shimada, Tatsuo, 2005. Skin morphology and its mechanical properties associated with loading. In: Pressure Ulcer Research. Springer, pp. 161–185.

Han, Tae-hee, Yoh, Jack J., 2010. A laser based reusable microjet injector for transdermal drug delivery. J. Appl. Phys. 107 (10), 103110.

Han, Tae-hee, Hah, Jung-moo, Yoh, Jack J., 2011. Drug injection into fat tissue with a laser based microjet injector. J. Appl. Phys. 109 (9), 093105.

Hogan, Nora C., Taberner, Andrew J., Jones, Lynette A., Hunter, Ian W., 2015. Needle-free delivery of macromolecules through the skin using controllable jet injectors. Expert Opin. Drug Delivery 12 (10), 1637–1648.

Kiyama, Akihito, Tagawa, Yoshiyuki, Ando, Keita, Kameda, Masaharu, 2016. Effects of a water hammer and cavitation on jet formation in a test tube. J. Fluid Mech. 787, 224–236.

Kiyama, Akihito, Endo, Nanami, Kawamoto, Sennosuke, Katsuta, Chihiro, Oida, Kumiko, Tanaka, Akane, Tagawa, Yoshiyuki, 2019. Visualization of penetration of a high-speed focused microjet into gel and animal skin. J. Visualiz. 22 (3), 449–457.

Krizek, Jan, Delrot, Paul, Moser, Christophe, 2020. Repetitive regime of highly focused liquid microjets for needle-free injection. Sci. Rep. 10 (1), 1–9.

Hiroshi Miyazaki, Shingo Atobe, Takamasa Suzuki, Hiromitsu Iga, and Kazuhiro Terai. Development of pyro-drive jet injector with controllable jet pressure. Journal of pharmaceutical sciences, 2019.

Onuki, Hajime, Oi, Yuto, Tagawa, Yoshiyuki, 2018. Microjet generator for highly viscous fluids. Phys. Rev. Appl. 9 (1), 014035.

Padilla-Martinez, J.P., Ramirez-San-Juan, J.C., Korneev, N., Banks, Darren, Aguilar, Guillermo, Ramos-Garcia, Ruben, 2013. Breaking the rayleigh-plateau instability limit using thermocavitation within a droplet. Atom. Sprays 23(6).

Padilla-Martinez, J.P., Berrospe-Rodriguez, C., Aguilar, G., Ramirez-San-Juan, J.C., Ramos-Garcia, R., 2014. Optic cavitation with cw lasers: a review. Phys. Fluids 26 (12), 122007.

Park, Mi-ae, Jang, Hun-jae, Sirotkin, Fedir V., Yoh, Jack J, 2012. Er: Yag laser pulse for small-dose splashback-free microjet transdermal drug delivery. Opt. Lett. 37 (18), 3894–3896.

Park, Geehoon, Ashin Modak, N., Hogan, Catherine, Hunter, Ian W., 2015. The effect of jet shape on jet injection. In: 2015 37th Annual International Conference of the IEEE Engineering in Medicine and Biology Society (EMBC). IEEE, pp. 7350–7353.

Peters, Ivo R, Tagawa, Yoshiyuki, Oudalov, Nikolai, Sun, Chao, Prosperetti, Andrea, Lohse, Detlef, Meer, Devaraj van der, 2013. Highly focused supersonic microjets: numerical simulations. J. Fluid Mech. 719, 587–605.

Rastopov, Stanislav F., Sukhodolsky, Anatoly T., 1991. Sound generation by thermo-cavitation-induced cw laser in solutions. In: Optical Radiation Interaction with Matter, vol. 1440. International Society for Optics and Photonics, pp. 127–134.

Rodríguez, Carla Berrospe, Visser, Claas Willem, Schlautmann, Stefan, Rivas, David Fernandez, Ramos-Garcia, Ruben, 2017. Toward jet injection by continuous-wave laser cavitation. J. Biomed. Opt. 22 (10), 105003.

Rohilla, Pankaj, Marston, Jeremy O., 2019. In-vitro studies of jet injections. Int. J. Pharm. 568, 118503.

Römgens, Anne M, Rem-Bronneberg, Debbie, Kassies, Roel, Hijlkema, Markus, Bader, Dan L., Oomens, Cees W.J., van Bruggen, Michel P.B., 2016. Penetration and delivery characteristics of repetitive microjet injection into the skin. J. Controlled Release 234, 98–103.

Ruddy, Bryan P., Bullen, Chris, Chu, Joanna Ting Wai, Jeong, Soo Hee, Madadkhahsalmassi, Bahareh, McKeage, James W., Svirskis, Darren, Tingle, Malcolm D., Xu, Jiali, Taberner, Andrew J, 2019. Subcutaneous nicotine delivery via needle-free jet injection: a porcine model. J. Controlled Release 306, 83–88.

Sangeorzan, Bruce J., Harrington, Richard M., Wyss, Craig R., Czerniecki, Joseph M., Matsen III, Frederick A., 1989. Circulatory and mechanical response of skin to loading. J. Orthop. Res. 7 (3), 425–431.

Schramm-Baxter, Joy, Mitragotri, Samir, 2004. Needle-free jet injections: dependence of jet penetration and dispersion in the skin on jet power. J. Controlled Release 97 (3), 527–535.

Tagawa, Yoshiyuki, Oudalov, Nikolai, Visser, Claas Willem, Peters, Ivo R., Meer, Devaraj van der, Sun, Chao, Prosperetti, Andrea, Lohse, Detlef, 2012. Highly focused supersonic microjets. Phys. Rev. X 2 (3), 031002.

Tagawa, Yoshiyuki, El Nikolai Oudalov, A., Ghalbzouri, Chao Sun, Lohse, Detlef, 2013. Needle-free injection into skin and soft matter with highly focused microjets. Lab Chip 13 (7), 1357–1363.

Tagawa, Yoshiyuki, Yamamoto, Shota, Hayasaka, Keisuke, Kameda, Masaharu, 2016. On pressure impulse of a laser-induced underwater shock wave. J. Fluid Mech. 808, 5–18.

Thoroddsen, Sigurdur T., Takehara, K., Etoh, T.G., Ohl, C.-D., 2009. Spray and microjets produced by focusing a laser pulse into a hemispherical drop. Phys. Fluids 21(11), 112101.

Vaughan, C.L., 1982. Smoothing and differentiation of displacement-time data: an application of splines and digital filtering. Int. J. Biomed. Comput. 13 (5), 375–386.

Vogel, Alfred, Nahen, Kester, Theisen, Dirk, Noack, Joachim, 1996. Plasma formation in water by picosecond and nanosecond nd: Yag laser pulses. i. Optical breakdown at threshold and superthreshold irradiance. IEEE J. Sel. Top. Quantum Electron. 2 (4), 847–860.

Wood, Graeme A., Jennings, Les S., 1979. On the use of spline functions for data smoothing. J. Biomech. 12 (6), 477–479.

Yoh, Jack J, Jang, Hun-jae, Park, Mi-ae, Han, Tae-hee, Hah, Jung-moo, 2016. A bio-ballistic micro-jet for drug injection into animal skin using a nd: Yag laser. Shock Waves 26 (1), 39–43.